Modeling of anisotropic hyperelastic heterogeneous knitted fabric reinforced composites

Annie Morch, Laure Astruc, Jean-Francois Witz, François Lesaffre, Pauline Lecomte-Grosbras, Damien Soulat, Mathias Brieu

Modeling of anisotropic hyperelastic heterogeneous knitted fabric reinforced composites

Annie Morch[a,*], Laure Astruc[a], Jean-François Witz[a], François Lesaffre[a], Pauline Lecomte-Grosbras[a], Damien Soulat[b], Mathias Brieu[a]

[a] *Univ. Lille, CNRS, Centrale Lille, FRE 2016 - LaMcube - Laboratoire de mécanique multiphysique multiéchelle, F-59000 Lille, France*

[b] *ENSAIT, Roubaix, France*

Abstract

Knitted fabrics are used to manufacture soft implants for medical applications. Once integrated in the body, the fabric forms a new composite material with the native and scar tissues. The mechanical behavior of the composite is assumed to be hyperelastic to match with the physiological behavior of the native tissues and thus to improve the fabric *in vivo* integration. Being able to predict the mechanical behavior of the composite regarding the tissue nature and the textile properties would accelerate the choice of the appropriate knit.

We propose an approach for modeling the mechanical behavior of an hyperelastic material reinforced by a knitted fabric. The main idea of the modeling approach described in the present paper is to couple micro or meso-structural observations with mechanical considerations. Knitted fabric composites display oriented and periodic microstructures. Since most knitted fabrics present a non-linear anisotropic mechanical behavior, the hyperelastic directional formalism seems appropriate to model the reinforced elastomer.

This work focuses on the development of a new directional model for the mechanical representation of anisotropic knitted fabric reinforced elastomers. The material is described with the help of a discrete network of directions that contribute distinctively to the material's global behavior. Experimental data obtained on reinforced elastomer composites were used to confirm the accuracy of the results as well as the prediction capabilities of the model. It seems able to represent an anisotropic stress answer of microstructured composite in uniaxial tension.

Keywords: composite, knitted fabric, rubber-like materials, anisotropy, network model, hyperelasticity, uniaxial tension, strain energy density, constitutive modeling

Introduction

Because their physical and mechanical properties may be close to the soft biological tissues, textile implants are widely used for medical applications [1]. Since the 1960s [2], the use of a textile reinforcement for the treatment of abdominal hernia has become popular, leading to an improvement in the surgical cure [3] and its success rate. The use of meshes has been then extended to various soft tissues reinforcement: for example vascular, abdominal [4] or even pelvic surgery [5]. Knitted fabrics are foremost preferred because they are highly flexible and do not easily fray [6], they also offer a broad range of structures and associated mechanical behaviors.

Following the implantation, the healing process of the biological tissues in contact with the textile implant, takes place, going together with the growth and colonization of scar tissues around the mesh [7]. A new composite made of the implant, the native and healed tissues replaces the initial native tissues and

*Corresponding author : annie.morch@gmail.com

should provide a non-pathological physiological behavior. In order to design the appropriate pattern, the development of new knitted fabrics goes usually through a "trial and error" process, combined with extensive animal studies. In order to shorten the progress towards the adapted textile - i.e. a textile that provides an adequate mechanical behavior to the composite, one needs to better understand and model the influence of the mesh on the mechanical behavior of the composite.

Soft connective tissues can support large deformations, and are supposed to be nearly incompressible due to their high water content [8, 9, 10, 11, 12]. According to their role in the body, they might present a different anisotropy ratio: from highly anisotropic, e.g. the abdominal rectus sheaths and linea alba [13, 14], to quasi isotropic, as illustrated by Rubod et al. [15] for the vaginal tissues. The mechanical behavior of such materials can be expressed in the frame of hyperelasticity in a way similar to rubber-like materials [11]. Knitted textiles, on the other hand, are highly porous structures made from the patterned and periodic interlooping of yarns. They usually display large deformations and a non linear behavior. In an attempt to model the mechanical behavior of the composite constituted of a knitted mesh and a rubber-like material, the modeling method requires to manage anisotropic and hyper-elastic behavior.

Microscale models are frequently used to represent the mechanical behavior of knitted fabric composites [6, 16, 17, 18]. The main literature focuses on knitted composites in the linear elasticity framework, see amongst others [19, 20, 21]. Huang et al. [22] developed a micromechanical model for the modeling of a polyurethane matrix reinforced with an interlock knitted fabric. He was able to represent an anisotropic and non linear mechanical behavior in two directions ; even if it appears that the modeling was not completely in agreement with the experimental data in one of the two tested directions. The micromechanical modeling approach relies on the definition of a unit cell, or a representative volume element, which comes down to the yarn loop. The aforementioned study focused on a plain knitted fabric. For meshes and more intricate knit patterns, the unit cell is not trivial to define, and tends to increase the computation time and number of modeling parameters, which could be a limitation to its application.

Micro-macro homogenization schemes [23, 24, 25] are able to represent the mechanical behavior of non linear composites. However, the large number of mechanical parameters, as well as interaction and boundary conditions, increase CPU-time and may limit their use. Simple approaches with a limited number of parameters are often preferred for hyperelastic material modeling. These models are based on macroscopical energy densities. In the literature, one finds two main types of strain energy densities, whether applied to rubber-like or biological materials. The first class consists of invariant based strain energy densities, either isotropic [26, 27] or anisotropic [28, 29]. Assuming the dry fabric is a continuous anisotropic material, a few models use a continuous macroscopical strain energy density to represent the non linear anisotropic behavior of the textile [30, 31, 32]. Yet, these continuous strategies raise some questions as the stress and strain measurements are not trivial for discrete structures. Moreover, a continuous model fails to report on the inner mobilities and realignment mechanisms occurring in the knitted fabric. In the composite, the elastomer presence impairs the natural mobilities of the textile. The strain energy density of the composite is therefore expressed from the two continuous energy densities of each material with an additional matrix-fiber energy density [33, 34, 35], depending on the embedding matrix mechanical properties and the textile fiber orientations. These models require generally an extended number of mechanical parameters, therefore a lot of experimental testing for their identification.

Besides these phenomenological models, network approaches offer micromechanically based models for the modeling of hyperelastic materials [36, 37, 38, 39]. They consist in a micro-macro homogenization based on a physical description of the material structure. The material is described as a network of macromolecular chains. The global strain density is obtained through the integration over a unit sphere surface of elementary chain densities [37]. These models are often referred to as micro-sphere [40] or directional models [41].

Different discrete integration schemes [42, 43, 44, 45] have been used over the years to simplify the computation. These models can represent the Müllins induced anisotropy, the softening process along specific directions for rubber-like materials [41, 46, 47, 48, 49]. Using an enriched micro-sphere approach, Raina and Linder [50] modeled the mechanical behavior of non woven materials. In their approach, fibers behave as linear isotropic materials. Taking into account the re-orientation variation and initial undulation of the fibers in a network model leads to an accurate representation of the mechanical behavior of non-woven samples under different solicitations.

Applications are also numerous for biological tissues [51, 52, 53, 54, 12]. Brieu et al. [12] presented an adapted version of this approach to model the mechanical behavior of isotropic connective tissues, with respect to the elastin and collagen fibers orientations, mechanical properties and volume fractions. Alastrué et al. [53, 55], Sáez et al. [56] worked with a microsphere approach to model the behavior of blood vessels : the use of different orientation distribution functions (ODF), based on the tissue microstructure, allows to define and weight preferential anisotropy directions.

Since this formalism is already used for the modeling of oriented hyperelastic materials and fibrous materials, we propose in this study an extended approach for modeling the mechanical behavior of anisotropic knitted fabric reinforced elastomers. Combining textile architectural considerations with the mechanical properties of the two constituents, this rather "meso"-sphere approach is able to model the anisotropic mechanical behavior of the composite. In the present paper, the initial microstructure defines a Lagrangian direction network, the anisotropy is induced by modifying the mechanical properties of each direction with regards to its constituent, i.e. if it belongs to the fabric or the matrix part of the composite.

The first section details the knitted fabric reinforced elastomer composites manufactured and studied in this work and briefly states the experimental results obtained after mechanical testing. The second part focuses on the modeling framework: the strain energy density is built according to the material's architecture. The last part of this paper validates the model, comparing the modeled and experimental behavior of the aforementioned composites. The predictive abilities of the mechanical model are finally assessed: the mechanical response of the composite is extrapolated from the mechanical behavior of its constituents.

1. Experiments - Knitted fabric composites

1.1. Materials

For the purpose of this study, composite plates were made of knitted fabric reinforced elastomer resins. The composites consist in 7 mm thick plates, where the fabric is embedded in the median plane of the matrix. Textile thickness ranged from 0.27 mm to 0.56 mm according to norm NF-EN-5084 [57], allowing at least 3.2 mm of plain elastomer matrix in the composite on either side. Altogether, six composite plates were manufactured, combining two different knitted fabrics and three elastomer materials. In addition to the composite plates, pure matrix sheets of each elastomer material, with the same dimension, were manufactured. Composite constituents are described separately below.

Three elastomer resins were chosen as bulk materials. In the following, they will be named respectively R (Essil 291, *Axson Technologies*), M (Sorta-Clear® 37 + 20 % Silicon Thinner®, *Smooth-on*) and S (Dragon Skin® FX-Pro, *Smooth-On*). Their respective mechanical strain-stress responses under uniaxial tension are shown in Figure 1. The mechanical characterization exhibited as well the incompressibility and isotropy of these materials. Each one exhibits a quasi linear stress-strain relationship, easily modeled by a second-order Yeoh law [27]. Table 1 presents the mechanical properties of each resin.

Two knitted fabrics with different patterns as well as mechanical apparent properties were chosen to manufacture the composites. Figure 2 illustrates the architectures of knitted fabrics T_1 and T_2. Each textile fabric (DYLCO, France) is manufactured from a 80 µm diameter monofilament polypropylene yarn. Average area densities of the fabrics are 48 g/m^2 for T_1 and 18 g/m^2 for T_2.

The dry textile mechanical behavior is characterized under uniaxial tension according to norm NF-EN-13934-1 [58]. Five samples of 5 cm in width and 20 cm in length are cut along warp and weft directions and mechanically tested in uniaxial tension at a displacement speed of 20 mm/min.

The mean force per unit width versus the elongation response is plotted for both textiles T_1 and T_2 in Figure 2 (a) and (b). It highlights the non-linearity as well as the anisotropy of the mechanical behavior between the two loading directions for each fabric, T_1 anisotropy ratio being higher than T_2[1].

[1]Given that the deformation mechanisms in the dry textile and in the composite cannot be easily correlated to each other, the experimental data gathered on the dry textile are not used for the modeling approach.

Name	Mechanical parameters	
	C_0 (MPa)	C_1 (MPa)
R	1.8×10^{-1}	2×10^{-2}
M	8.6×10^{-2}	3×10^{-3}
S	1.4×10^{-2}	7×10^{-4}

Table 1: Second-order Yeoh parameters for the elastomer matrices

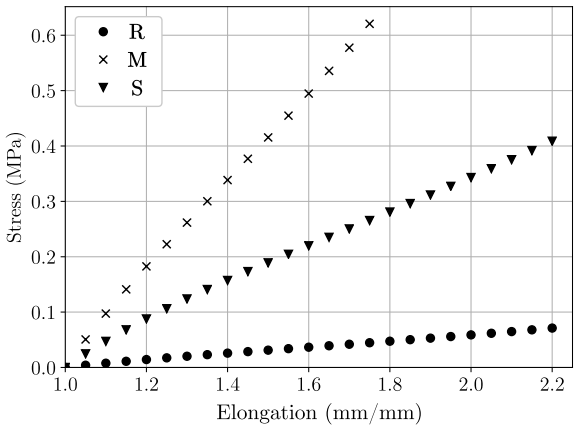

Figure 1: Stress vs strain mechanical answer for elastomer resins R, M and S.

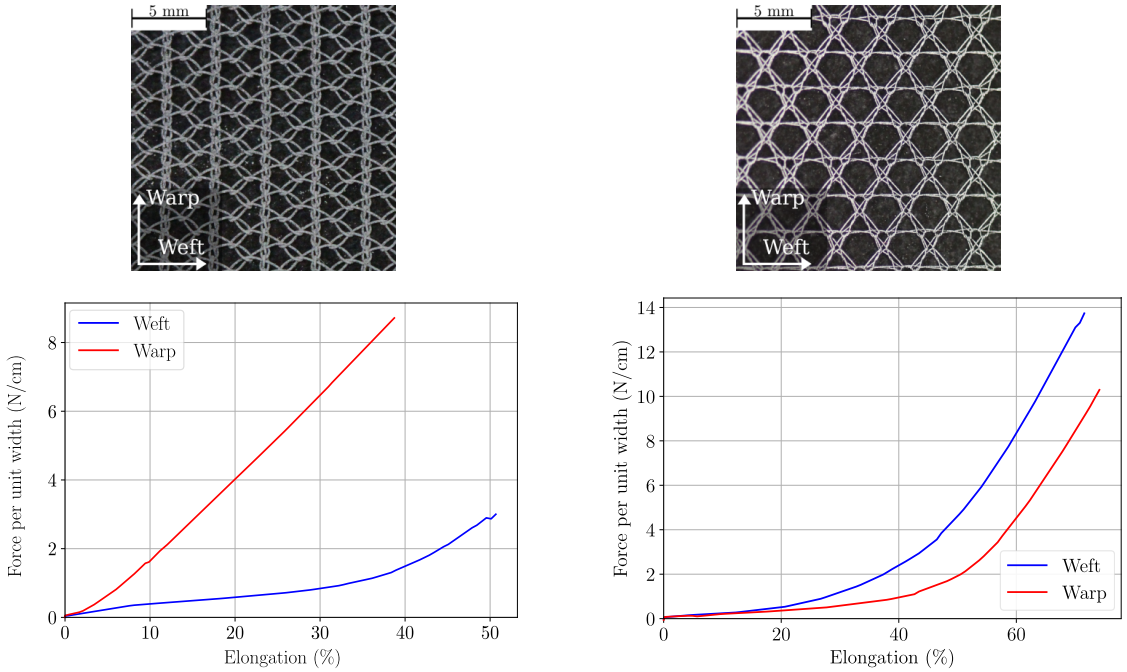

(a) **(b)**

Figure 2: Architecture and force per unit width vs deformation response under warp (red) and weft (blue) directions of dry textiles T_1 (a) and T_2 (b)

1.2. Composite mechanical characterization

Since the dry knitted meshes are anisotropic, composite samples are characterized in uniaxial tension along the two specific manufacturing directions. The loading directions are chosen to match with the warp and weft orientations of the textile. The displacement rate is set to 20 mm/min to meet textile normative standards (NF-EN-13934-1) [58]. Uniaxial tension tests are enhanced with cyclic loadings: the material is loaded at growing deformation levels and unloaded to 0.5 N. After a cycle, the sample is reloaded up to

the next deformation level, increased of 5 % for the composite and 10 % for the resin samples. Cycles are performed successively until the sample breaks or is severely damaged. Figure 3 details the loading path in terms of strain and force limits and global stress/strain response.

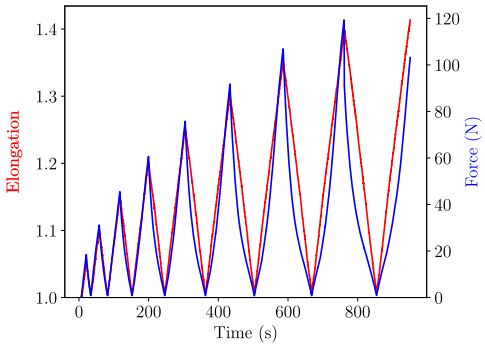

(a) Cyclic loading path in strain and force

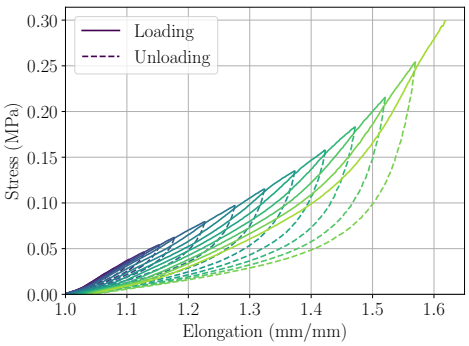

(b) Cyclic loading stress-strain answer of composite $S+T_1$

Figure 3: Cyclic loading: (a) Force and strain control limits of the cyclic testing regarding time ; (b) Stress vs strain behavior

Forces are measured with a 2 kN load-cell (sensitivity: 0.6 N). Video-extensometry is performed on the front of the sample: four black paint dots are dropped off on the sample surface, in order to compute both longitudinal and transverse deformations. Composites are punched in 5 cm length and 2 cm wide samples. These dimensions are considered to ensure the mechanical representativity of the material [59]. Thickness is measured with a caliper (precision : 0.02 mm) around 7 mm average.

The experimental results, illustrated in Figure 3(b) for the composite $S+T_1$, show the hysteresis between the loading and unloading parts as well as the discrepancy between the first and second load to a certain level of deformation. This softening phenomenon is known as the Müllins effect [60]. The hysteresis between load and unload is underlined in Figure 3(b): within the same color, solid and dotted lines stand respectively for the load and following unload. Similar observations are made on pure matrix samples or other composites. Diani et al. [61] proved, on a filled elastomer, that the viscous contribution appears to be less significant during an unloading phase than during a loading one. To ensure insignificant viscoelastic effects, it was therefore decided to only model the unload (dotted lines on Figure 3(b)). The identification of the proposed constitutive model is arbitrarily focused on the last unload curve, following the maximum stretch level, in order to model the behavior over the broadest range of deformations.

2. Mechanical modeling

Knitted fabrics present geometrical architectures. Due to the stiffness and anisotropy of the knitted fabrics, with respect to the isotropic elastomer resin, the mechanical properties of the newly formed composite come mainly from the fabric's structure. It seems relevant to base the mechanical model on microstructural considerations: a new model based on the directional formalism was developed.

2.1. Directional strain energy density

Directional models were first developed for hyperelastic, rubber-like materials. Such materials come from the reticulation of long macro-molecular chains, organized in a three-dimensional complex network. Each chain, described by its own strain energy density contributes to the material, i.e. the macro-molecular network, strain energy density. Treloar and Riding [37] expressed the strain energy density of an ideal

continuous distribution of chains. The global energy potential is written as the integration of each elementary energy density over the unit sphere surface:

$$W = \frac{1}{4\pi} \iint_S w(\underline{\mathbf{u}}) d\Omega \tag{1}$$

where the vector $\underline{\mathbf{u}} = (\cos(\theta), \sin(\theta)\cos(\phi), \sin(\theta)\sin(\phi))$ is defined by the spherical coordinates (θ, ϕ), and $d\Omega$ is the infinitesimal surface element $d\Omega = sin(\theta)d\theta d\phi$.

These models, developed for highly-deformable rubber-like materials, offer a wide-range of possibilities: isotropic or anisotropic behavior, strain softening (Müllins-effect), residual strains ...

Analytical computation can be time-consuming. For this reason, discrete distributions with a finite number of directions were introduced: 3-chain model [36], 8-chain model [38], and larger numerical integration schemes providing great precision of the estimated integrate [42]. In order to represent the possible anisotropy of the material behavior, new distributions based on the material preferential orientations were built up as well [41, 45].

The discretized strain energy density is expressed as a function of the elementary strain energy density w of each material direction $\underline{\mathbf{u}}^i$:

$$W(\underline{\underline{\mathbf{F}}}) = \sum_{i=0}^{n} \omega_i w \left(\frac{\nu_i}{||\underline{\mathbf{u}}^i||} \right) \tag{2}$$

with $||\underline{\mathbf{u}}^i||$ the norm of the material direction $\underline{\mathbf{u}}^i$, ω_i the integration weight associated to direction $\underline{\mathbf{u}}^i$ on the sphere surface, and w the elementary strain energy density. The previous integration schemes with preset directions cannot be used in our specific case as they cannot relate to the architecture of our composite. A custom integration scheme over the sphere surface was designed. Directions are set on the sphere surface according to the microstructure. The sphere is tiled with nine node quadrangles, on which a quadratic Lagrangian function q is integrated. The integration weights of node i (associated with direction i) is obtained by assembling the contribution of all the elements, in a similar way to the finite element method.

The scalar value ν_i represents the elongation seen by the chain in direction $\underline{\mathbf{u}}^i$. It is computed according to :

$$\nu_i = \sqrt{{}^t(\underline{\underline{\mathbf{F}}}.\underline{\mathbf{u}}^i)(\underline{\underline{\mathbf{F}}}.\underline{\mathbf{u}}^i)} \tag{3}$$

where $\underline{\underline{\mathbf{F}}}$ is the macroscopic transformation gradient tensor.

Directional models, designed for rubber-like material, are based on a non Gaussian statistical theory. The commonly used elementary density w requires the use of the inverse Langevin function [62]. Its expression depends on two physically relevant parameters : n^i and $\sqrt{N^i}$, respectively the i$^{\text{th}}$ chain density and limit of extensibility:

$$w(\nu_i) = n^i N^i kT \left[\beta \mathcal{L}(\beta) + \ln \left(\frac{\beta}{\sinh(\beta)} \right) \right] \tag{4}$$

where $\beta = \mathcal{L}^{-1}\left(\frac{\nu_i}{N^i}\right)$ and $\mathcal{L}(x) = \coth(x) - 1/x$ is the Langevin function.

Even under an approximate form (Taylor expansion, Padé approximant [63]), the use of non Gaussian statistics in the potential expression carries a strong interdependency of the two parameters n^i et N^i. As a result, it can impair the mechanical characterization.

The physical interpretation of $\sqrt{N^i}$ implies that this quantity is strictly larger than one : otherwise no sooner had the traction test begun than the sample chains already broke. In the specific case of the textile reinforced composite, a simplified parameter identification on the experimental data of R+T$_1$ composite was run. Assuming the isotropy of the composite, i.e. the same mechanical parameters for each chain within the material, mechanical parameters $n^i = n$ and $\sqrt{N^i} = \sqrt{N}$ were optimized to fit experimental data, leading to a non physical limit of extensibility $\sqrt{N} < 1$. Figure 4 shows the results of the optimization as well as the general shapes of stress evolution for admissible values of $\sqrt{N}$. To be able to fit the experimental data obtained and previously presented, this model has to allow for physically not admissible mechanical parameters.

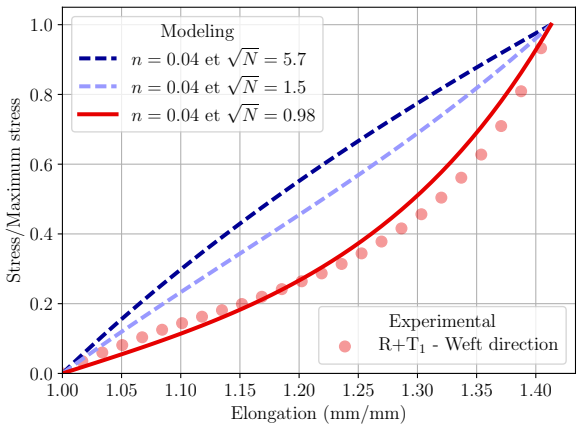

Figure 4: Evolution of the modeled normalized isotropic stress where the elementary density depends of the inverse Langevin function [62] with a constant chain density n and varying limit of extensibility $\sqrt{N}$. The experimental and modeled composite R+T$_1$ stress evolution stand in red dots and straight line respectively for the comparison.

The modeling law fails to represent properly the mechanical behavior of textile composite. It turns, at the best, into a phenomenological model with non physical parameters. In this specific case, it seems relevant to use a novel elementary potential to replace the inverse Langevin function. Similar to Carol et al. [64] or Lion et al. [65] with a directional Mooney-Rivlin chain density, the elementary energy density is inspired by a generalized Yeoh law [27], therefore expressed as:

$$w(\nu_i) = \sum_{k=1}^{n} a_k^i (\nu_i - 1)^k \tag{5}$$

The a_k^i coefficients are understandable as rigidities and expressed in MPa. Unlike the n^i and N^i they are fully independent.

According to the incompressibility assumption, the first Piola-Kirchhoff stress tensor is written:

$$\tau = \frac{\partial W}{\partial \underline{\underline{\mathbf{F}}}} - p\underline{\underline{\mathbf{F}}}^{-T} \tag{6}$$

where p is the Lagrange multiplier, or hydrostatic pressure. The partial derivative of the strain density regarding $\underline{\underline{\mathbf{F}}}$ is expressed as:

$$\frac{\partial W}{\partial \underline{\underline{\mathbf{F}}}} = \sum_{i}^{n} \omega_i \left(\sum_{k} k(a_k^i (\nu_i - 1)^{k-1}) \right) \frac{\underline{\underline{\mathbf{F}}} \underline{u_i} \otimes \underline{u_i}}{\nu_i} \tag{7}$$

For anisotropic materials, in order to avoid any residual stresses in an undeformed state, the partial derivative $\dfrac{\partial W}{\partial \underline{\underline{\mathbf{F}}}}$ is replaced by [41]:

$$\frac{\partial \widetilde{W}}{\partial \underline{\underline{\mathbf{F}}}} = \frac{\partial W}{\partial \underline{\underline{\mathbf{F}}}} - \left. \frac{\partial W}{\partial \underline{\underline{\mathbf{F}}}} \right|_{\underline{\underline{\mathbf{F}}}=\mathbf{1}} \tag{8}$$

2.2. Microstructure representation

Both elastomers and textile composites are going to be modeled with the directional model, developed in Subsection 2.1. To model the mechanical behavior of the composite, one needs to set the material discretization and integration network and determine the mechanical properties of each direction.

The network describing the material has two main goals: first, to perform the numerical integration over the sphere surface, and second, to induce possible privileged anisotropy directions. The directions set relies on the material microstructure or architecture. For isotropic materials, like silicon resins, the orientation distribution can be randomly chosen on the sphere surface. On the contrary, for an anisotropic composite, it is mandatory to introduce specific anisotropy directions, depending in the present study on the knitted textile microstructure.

For isotropic materials, the integration scheme relies on a network of 200 directions, evenly distributed on the sphere surface. The discretized sphere is plotted in Figure 5. The same directions set will be used for the modeling of any silicon resin. In an isotropic material, each direction displays the same mechanical parameters a_k, as mentioned in Equations 5 and 7. Pure matrix directions mechanical parameters can be obtained from full matrix sample characterization.

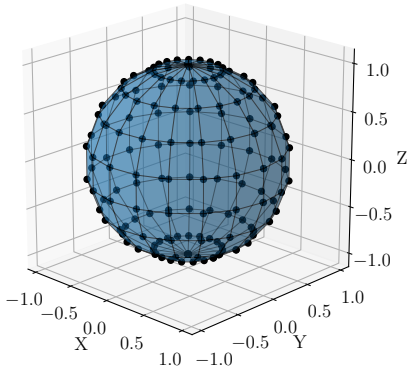

Figure 5: Example of the distribution of the material and integration directions for an isotropic material

On the contrary, textile parameters cannot be determined from dry textile samples. Textiles are discontinuous materials, the cross-section is thus not trivially measured or computed. The stress-strain relationship cannot be easily obtained. Moreover, a continuous strain energy density does not seem appropriate for modeling the textile mechanical response. Therefore, the fabric mechanical properties will be identified within the composite thanks to the directional approach and the discretization of the material directions.

In order to induce the anisotropy related to the textile embedded in the matrix, specific material directions can be differentiated, by applying variable mechanical parameters. The textile, inducing the anisotropic behavior of the composite, is located in the median plane of the sample. Outside this plane, the composite is constituted of pure matrix. Therefore, to describe a composite, two directions families will be used: "pure fiber" directions, along the textile fabric architecture, and "pure matrix" directions elsewhere. This distribution assumes that each direction family is independent from the other. More importantly, it means that the textile mechanical properties are independent from the matrix used for manufacturing of the composite.

For reasons of symmetry, either in the T_1 or T_2 composite, the material is described with three types of directions, illustrated in Figure 6:

- "pure fibers" directions located in the median plane following the textile principal orientations. For reasons of symmetry, two types of directions are picked out : Type I fibers, illustrated in blue and Type II fibers, highlighted in red in Figure 6(a) and (b) ;
- and "pure matrix" directions, N directions, featured in black (Figure 6(c), and (d)), evenly distributed in the median plane between the fibers' directions, and outside on the rest of the unit sphere surface.

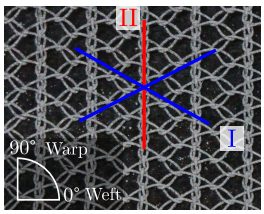

(a) Red and blue lines outline the two fibers family in T_1, respectively along 90° and 30° to the weft direction

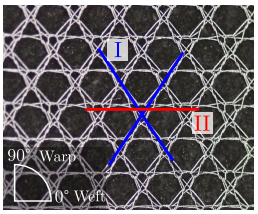

(b) Red and blue lines outline the two fibers family in T_2, respectively along 0° and 55° to the weft direction

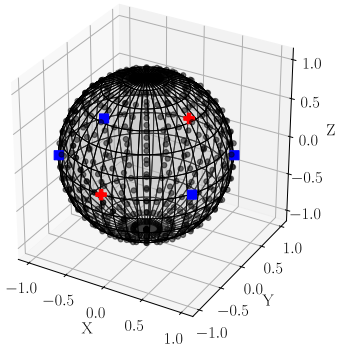

(c)

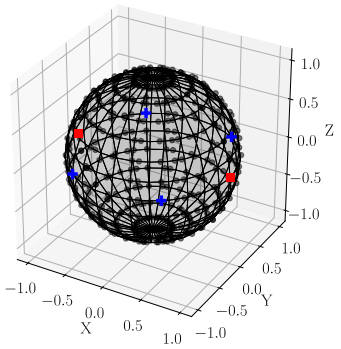

(d)

Figure 6: (a) and (b) Close view of the median plane fibers directions respectively for textile T_1 and T_2. (c) and (d) 3D representation of the composite directions distributed to evenly discretize the sphere surface.

2.3. Model implementation

Since the transformation gradient tensor components are not all measurable (particularly the in-plane cross-sectional shear strains) in the anisotropic composite, the volume variation cannot be estimated. In order to simplify the problem, we assume that the textile does not impair the incompressibility of the matrix ; the composite is therefore assumed to be incompressible.

Since the transverse deformation along the thickness of the sample is not known, the gradient transformation tensor is estimated as : $\underline{\underline{\mathbf{F}}} = \mathrm{diag}(F_{11}, F_{22}, \frac{1}{F_{11}F_{22}})$ to ensure the incompressibility of the material [41].

In order to speed up the mechanical parameter identification, we assume a more simple elementary density than the general form, expressed as :

$$w_i = a_0^i(\nu_i - 1) + a_4^i(\nu_i - 1)^5 \tag{9}$$

where a_0^i, a_4^i and ν_i are respectively the mechanical parameters and the deformation along Direction i, computed from Equation 3. Alternative densities with intermediate polynomial orders were tested but did not significantly change the mechanical behavior modeling, while the computation time during the mechanical parameters identification highly increased. The density is therefore simplified and reduced to only two polynomial orders, which were considered to be sufficient for the representation of the mechanical behavior.

For silicon matrix samples, one set of two parameters $\{a_0^m, a_4^m\}$ is consequently enough to model the entire behavior of the material. In a composite sample, "pure matrix" directions are assumed to act like the directions of the full resin samples. Similarly to Alastrué et al. [53], "pure fiber" directions are supposed to behave like cords: a fiber direction contributes to the overall stress only when submitted to a traction solicitation. If a fiber direction undergoes compression loading, the direction will behave as if it were made of pure matrix.

Under small deformations, the embedded textile fibers are supposed to realign with the traction direction. Composites seem indeed to behave like full elastomer samples in that range, as suggested for composite M+T_1

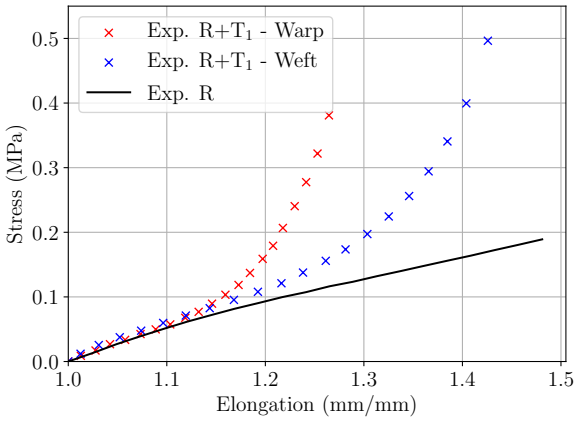

Figure 7: Mechanical stress response in uniaxial tension of matrix M and composite M+T_1 under warp and weft directions

in Figure 7. Therefore, the preponderant mechanical parameter in small deformations is set equal to the matrix : $a_0^{fiber} = a_0^m$. The strain energy density of a fiber direction is written as a function w_i^f depending on one fiber mechanical parameter a_4^f:

$$w_i^f = \begin{cases} a_0^m(\nu_i - 1) + a_4^f(\nu_i - 1)^5 \text{ when } \underline{\underline{\mathbf{F}}}.\underline{u_i} > 1 \text{ (fiber direction in traction)} \\ a_0^m(\nu_i - 1) + a_4^m(\nu_i - 1)^5 \text{ when } \underline{\underline{\mathbf{F}}}.\underline{u_i} \leq 1 \text{ (fiber direction in compression)} \end{cases} \tag{10}$$

The optimization of the mechanical parameters is obtained through the minimization of the error between the experimental and modeled stress tensor components. The minimization is performed with a genetic algorithm, the differential evolution algorithm [66] that finds the global minimum of a multivariate function, available in Python library Scipy [67].

3. Results

With the help of the modeling framework, set in the previous section, and experimental data on full matrix and composite samples, the mechanical properties of respectively "pure" matrix and "pure fibers" directions are determined. The model implementation and optimization is performed in Python with the help of the Numpy and Scipy libraries [67, 68].

3.1. Mechanical properties identification

Table 2 and Figure 8 summarize the results of the identification process of the pure matrix parameters. The fit stands close to the experimental results whichever resin sample. The directional strain energy density is still relevant for isotropic materials as it does not increase the number of mechanical parameters in comparison with a second-order Yeoh law.

Resin	Mechanical parameters	
	a_0^m (MPa)	a_4^m (MPa)
R	2.83	6.88
M	1.84	0.54
S	0.31	0.04

Table 2: Identified mechanical parameters of the directional model for each resin.

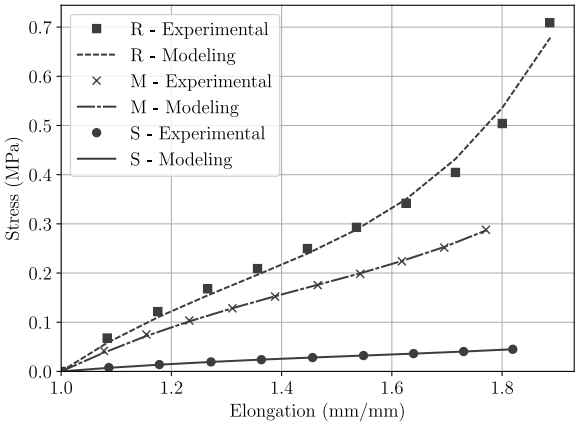

Figure 8: Experimental and modeled plots of the stress-strain behavior of resins R, M and S under uniaxial tension.

According to the proposed approach, the "pure matrix" mechanical properties in the composite are the same as in the full-matrix samples. Therefore, only the "pure fibers" mechanical properties needs to be identified in order to model the mechanical behavior in warp and weft directions. The textile mechanical parameters should remain identical whatever the silicon resin. One set of mechanical parameters, $\{a_4^I, a_4^{II}\}$ per fabric should allow the modeling of the three composites, made with the relevant textile, in warp or weft orientation of the solicitation. The unique set is obtained while minimizing at the same time the error between modeled and experimental data for the three composites and two orientations of solicitation.

Figures 9 and 10 display the experimental and modeled plots after the optimization of fabric T_1 and T_2 mechanical parameters respectively.

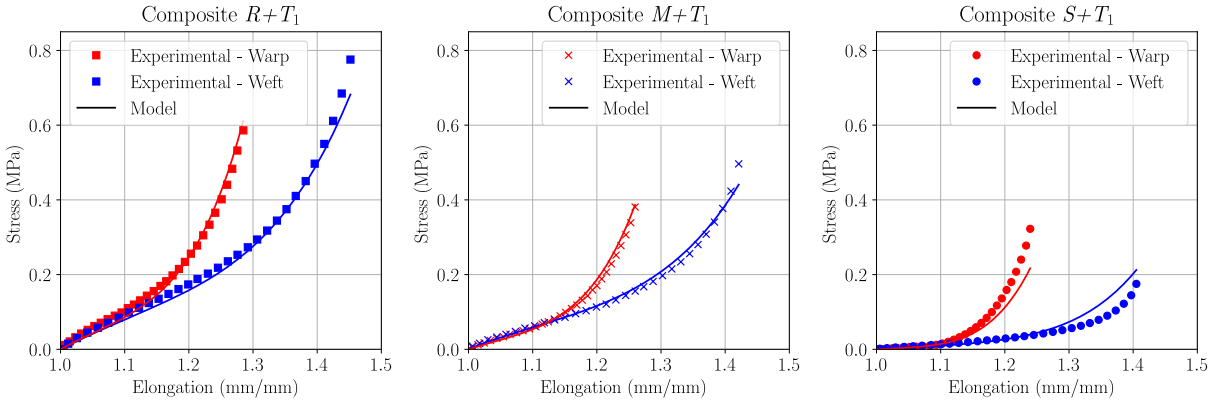

Figure 9: Experimental (dotted) and modeled (straight lines) plots of the mechanical behavior in uniaxial traction in warp and weft orientations of composites made of textile T_1 and silicon resins : from left to right R, M and S. The textile parameters are $a_4^I = 6.9 \times 10^2$ MPa and $a_4^{II} = 2.0 \times 10^3$ MPa.

For each textile, the minimization converges toward a unique set of mechanical coefficients $\{a_4^I, a_4^{II}\}$, that is able to represent both the anisotropic behavior within the same composite and, according to the embedding resin, the shape of the mechanical answer of the three materials. Mean relative errors between the modeled and experimental stress signal are quantified for each composite. Composites R+T_1 and M+T_1 are well approximated with respective mean errors of about 13% and 11% along the warp direction and 7% or 9% along the weft direction. The modeling of composite S+T_1 is less effective with mean relative errors around 30% in both directions.

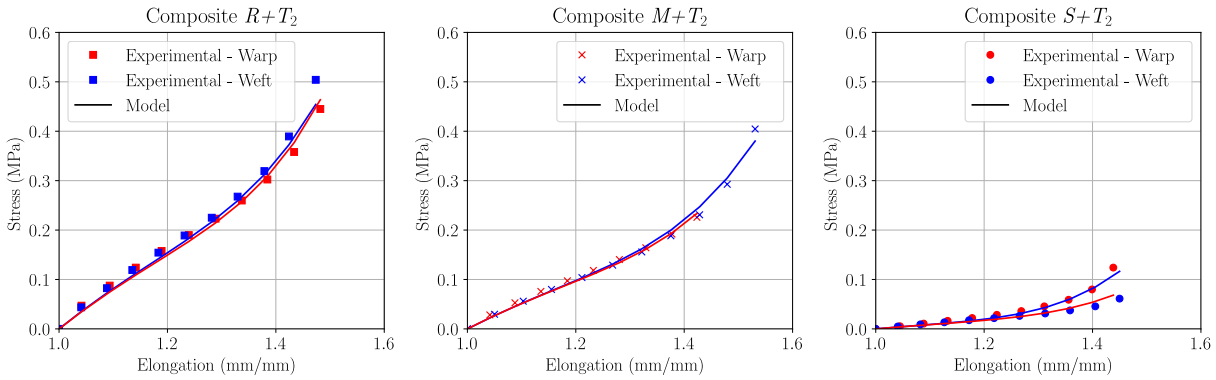

Figure 10: Experimental (dotted) and modeled (straight lines) plots of the mechanical behavior in uniaxial traction under warp and weft orientation of composites made of textile T_2 and silicon resins : from left to right R, M and S. The textile parameters are $a_4^I = 1.4 \times 10^2$ MPa and $a_4^{II} = 7.5 \times 10^2$ MPa.

The model identification shows similar efficiency and mean errors on composites reinforced with T_2. Mean errors go up to 8% in both directions for R+T_2 and M+T_2 while reaching 30 to 35% respectively along warp and weft directions in S+T_2. Figure 10 shows indeed the non-ideal fit of the composite S+T_2. The fiber parameters were identified by minimizing the error between the modeled and experimental stresses of the three composites at the same time. The contributions to the error function are much more important given the stress levels for the composites R+T_2 and M+T_2 than for S+T_2, given the lower rigidity of resin S. That could explain the non-ideal fit. This would also explain the poorer fit in composite S+T_1 compared to R+T_1 and M+T_1. In addition, the weft and warp direction experimental responses showed opposite behavior compared to composites R+T_2 and M+T_2. This is another bias that could be responsible for the poor modeling fit.

With such polynomial directional law, the mechanical behavior of structured anisotropic materials is represented accurately, based on a relevant description of the material microstructure and only two mechanical parameters.

3.2. Prediction

Method

The previous sections, dealing with the parameter identifications, highlighted the independence of the silicon and textile mechanical parameters for composites made of the same textile and different bulk elastomers. It would be interesting, knowing the textile and a new silicon separately, to predict the behavior of the composite manufactured from these two components.

The textile fiber parameters can only be identified with the help of a composite constituted of the fabric embedded in an elastomer bulk. The model formalism is indeed not appropriate for non-continuous material such as dry knitted fabric.

In a prediction context, only the mechanical parameters a_k^i and the evolution of the longitudinal strain F_{11} are known *a priori*. In order to predict the stress response τ_{11} under uniaxial tension according to Equation 6, additional input variables are required to run the model: the other diagonal components of the gradient transformation tensor $\underline{\underline{\mathbf{F}}}$, precisely how F_{22} and F_{33} evolve regarding the axial stretch, and finally the Lagrange multiplier p, to enforce incompressibility.

From the diagonal form of the gradient transformation tensor and the incompressibility assumption, the expression of F_{33} only depends on F_{11} and F_{22}: $F_{33} = \dfrac{1}{F_{11}F_{22}}$. The stress tensor, modeled according to Equation 6, leads to a system of three equations and three unknown variables: τ_{11}, the axial stress, F_{22} the transverse strain, and p the Lagrange multiplier. In a first step, the transverse deformation F_{22} and p can

be obtained from the resolution of $\tau_{22} = \tau_{33} = 0$ in uniaxial tension:

$$\begin{cases} \tau_{22} = 0 = \sum_{i=0}^{n} \left(a_0^i + 5a_4^i(\nu_i - 1)^4\right) \frac{F_{22}u_2^i}{2\nu_i} - \frac{p}{F_{22}} \\ \tau_{33} = 0 = \sum_{i=0}^{n} \left(a_0^i + 5a_4^i(\nu_i - 1)^4\right) \frac{F_{33}u_3^i}{2\nu_i} - \frac{p}{F_{33}} \end{cases} \tag{11}$$

with $\nu_i = \sqrt{(F_{11}u_1^i)^2 + (F_{22}u_2^i)^2 + (F_{33}u_3^i)^2}$

Knowing F_{22} and p, the longitudinal stress is estimated in a second step:

$$\tau_{11} = \sum_{i=0}^{n} \left(a_0^i + 5a_4^i(\nu_i - 1)^4\right) \frac{F_{11}u_1^i}{2\nu_i} - \frac{p}{F_{11}} \tag{12}$$

This two-step prediction method is applied on composites made from textile T_1 or T_2. In the following, the fiber mechanical parameters will be identified either from a single composite or two composites at the same time rather than on the three composites simultaneously. These parameters are then used to predict the behavior of the remaining one(s).

Results

The mechanical parameters of T_1 fibers are identified only in composites S+T_1 and R+T_1 separately in order to model composite M+T_1. Their values might vary slightly depending on the composite used for the characterization, as shown in Table 3. Fitting curves, displayed on Figure 11(a) and (b) seem closer to the experimental results as the optimization is indeed less constrained than in Subsection 3.1.

Composite	Mechanical parameters	
	a_4^I (MPa)	a_4^{II} (MPa)
R+T_1	785	1781
S+T_1	430	1796

Table 3: Mechanical parameters of the textile fiber directions as identified in composites R+T_1 and S+T_1

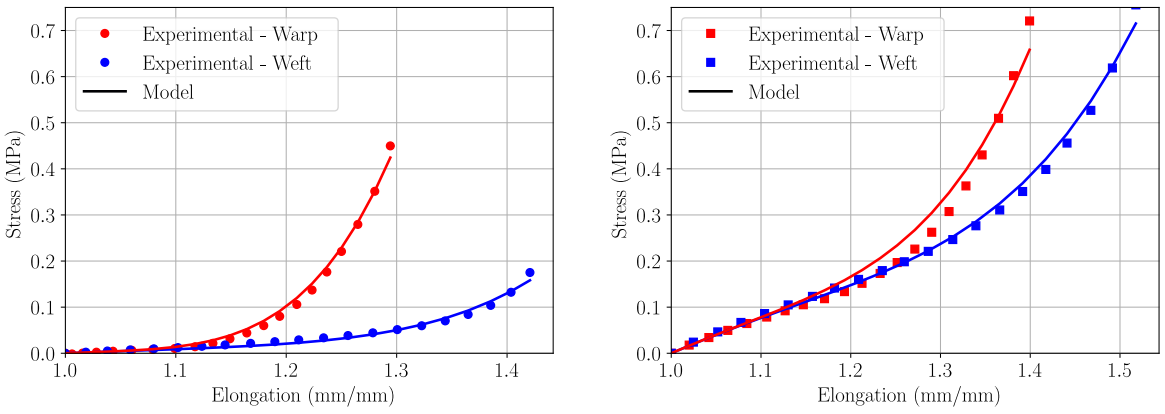

(a) **(b)**

Figure 11: Experimental and modeled curves of composites S+T_1 (a) and R+T_1 (b).

The prediction can be achieved, while performing the two-step process described in the previous paragraph, for each parameter set. Trend lines are therefore computed, creating a prediction range of the

composite M+T_1. As seen in Figure 12, the prediction range surrounds the experimental results. The identification of the fiber mechanical parameters on R+T_1 and S+T_1 concurrently may fairly improve the predicted response. The conjectured warp and weft behavior, plotted in straight lines on Figure 12, stands closer to the experimental results.

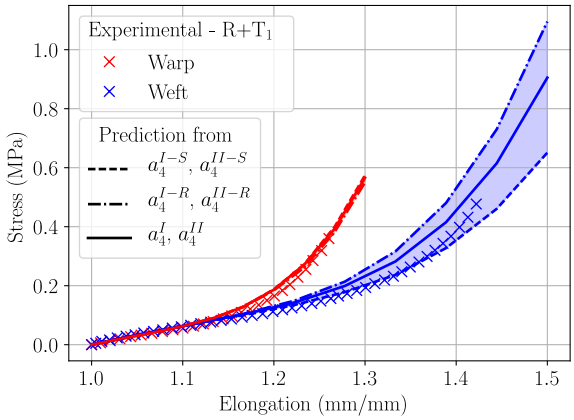

Figure 12: Prediction range of the mechanical behavior of composite M+T_1 in uniaxial tension under warp and weft directions.

The robustness of the prediction is assessed when permuting the identified and predicted composites. Figure 13(a) and (b) shows the predicted behavior of composites R+T_1 and S+T_1 respectively. While the prediction abilities are satisfying when looking at the more rigid composite, they are not as good for the softest composite S+T_1. This could come from the higher gap in the mechanical properties of the elastomer resin S compared to the two others. This is the main limitation: the model can be used as an effective predictive tool when the embedding material is chosen in a close range to the resin of the known composites.

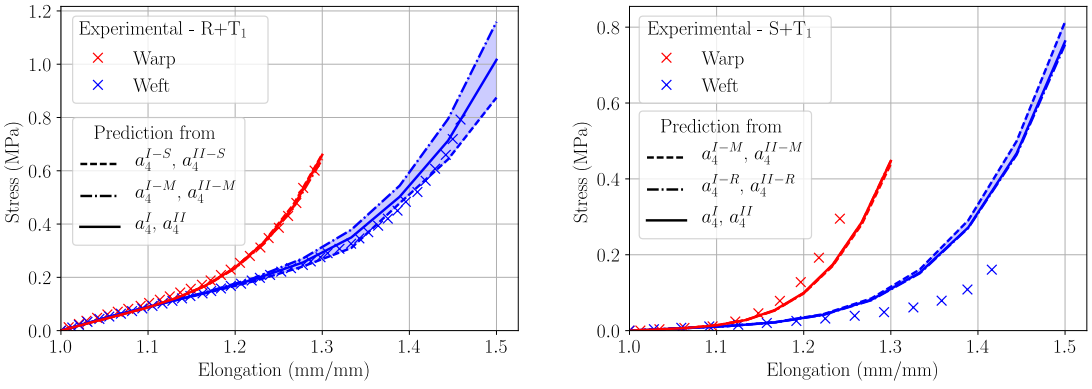

(a) **(b)**

Figure 13: Prediction range of the mechanical behavior of composites R+T_1 (a) and S+T_1 (b) in uniaxial tension under warp and weft directions.

In a similar way, the predicted behavior is computed for composite constituted of textile T_2. The predicted behavior is compared to the experimental results in Figure 14. In a similar way, a modeled range surrounds the experimental data, showing the efficiency of the prediction.

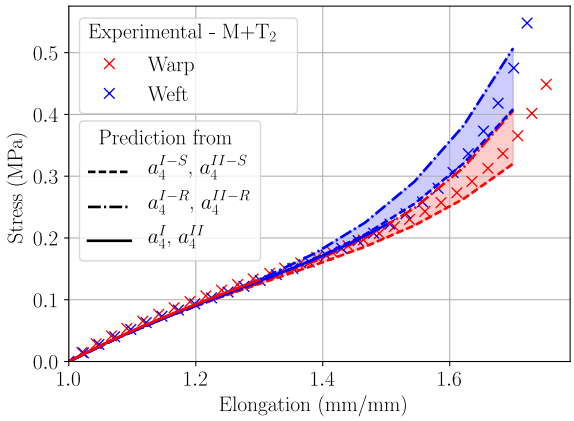

Figure 14: Prediction range of the mechanical behavior of composite M+T$_2$ in uniaxial tension under warp and weft directions.

4. Conclusion

A simple directional model was developed for the modeling of knitted textile reinforced composites. The directional formalism takes into account privileged directions of anisotropy based on a description of the microstructure. The polynomial directional elementary density keeps the physical meaning of every parameter: each direction is associated with its own rigidity parameters. The present study focused on the validation of this model for two different textiles embedded in rubber-like materials. The model is able to correctly represent the stress response of composites made with two textiles in uniaxial tension. It can also be used as a predictive tool, when both the matrix and textile mechanical parameters are known. However, in order to provide a reliable prediction, it seems necessary to study a resin material in the range of those used during the identification. Without additional data or observations, this remains the main limitation of the present study.

The results obtained in terms of identification or prediction were less effective for the softer composite. The deformation mechanisms of the composite on the one hand, and in the knitted fabric on the other hand, were not investigated. Full-field measurements during the test could provide a better understanding of the mobilities, fiber rearrangement or deformations occurring during the loading. Information about the deformation mechanisms should also help to refine the modeling approach.

In the present work, the interactions between the fiber directions, due to the interlooping of the yarn and structure of the textile, were neglected. Using coupling parameters might be an improvement for the representation of the mechanical behavior of the composite, especially when the matrix leads to large deformations. It may also be mandatory when using this model in different loading configurations.

The modeling approach was indeed only validated on uniaxial loading cases. The uniaxial loading was considered because of its wide use in biological tissue testing. However, besides its poor mechanical representativity with regards to physiological solicitations, uniaxial tension fails to represent the coupling effects that might happen during multi-axial testing. Further work should focus on the modeling or prediction of different loading conditions: multi-axial, or additional loading directions under uni-axial tension for example.

The last perspective of this work is aimed at developing a damage model: the aforementioned composites presented a damageable behavior with a strong Müllins effect. The cyclic loading results should also be used to improve the model with damage parameters capable to model the evolution of the residual stress evolution, as well as the rigidity loss with the maximum strain seen by the material.

Acknowledgements

The authors would like to express their gratitude to the company DYLCO (Bertry, France) and its plant manager Thierry Mériaux for manufacturing and providing all the knitted fabrics used in the present study. The authors thank the French Agence Nationale de la Recherche (ANR-13-TECS-0003-01) for the financial support of this study.

References

[1] Y. Qin, Applications of advanced technologies in the development of functional medical textile materials, 2016. doi:10.1016/B978-0-08-100618-4.00005-4. arXiv:arXiv:1011.1669v3.

[2] F. C. Usher, A new plastic prosthesis for repairing tissue defects of the chest and abdominal wall, The American Journal of Surgery 97 (1959) 629–633.

[3] J. W. A. Burger, R. W. Luijendijk, W. C. J. Hop, J. A. Halm, E. G. G. Verdaasdonk, J. Jeekel, T. N. Pappas, C. E. Lucas, C. A. Pellegrini, D. W. Easter, J. E. Fischer, S. J. Mathes, L. W. Way, H. T. Debas, R. S. Jones, Long-term follow-up of a randomized controlled trial of suture versus mesh repair of incisional hernia, Annals of Surgery 240 (2004) 578–585.

[4] R. W. Luijendijk, W. C. Hop, M. P. van den Tol, D. C. de Lange, M. M. Braaksma, J. N. IJzermans, R. U. Boelhouwer, B. C. de Vries, M. K. Salu, J. C. Wereldsma, C. M. Bruijninckx, J. Jeekel, A Comparison of Suture Repair with Mesh Repair for Incisional Hernia, New England Journal of Medicine 343 (2000) 392–398.

[5] V. Bot-Robin, J.-P. Lucot, G. Giraudet, C. Rubod, M. Cosson, Use of vaginal mesh for pelvic organ prolapse repair: a literature review, Gynecological Surgery 9 (2011) 3–15.

[6] T. D. Dinh, O. Weeger, S. Kaijima, S. K. Yeung, Prediction of mechanical properties of knitted fabrics under tensile and shear loading: Mesoscale analysis using representative unit cells and its validation, Composites Part B: Engineering 148 (2018) 81–92.

[7] J. M. Bellón, J. Buján, L. Contreras, A. Hernando, Integration of biomaterials implanted into abdominal wall: process of scar formation and macrophage response, Biomaterials 16 (1995) 381–387.

[8] G. A. Holzapfel, T. C. Gasser, R. W. Ogden, A New Constitutive Framework for Arterial Wall Mechanics and a Comparative Study of Material Models, Journal of Elasticity 61 (2000) 1–48.

[9] C. Rubod, M. Boukerrou, M. Brieu, J.-C. Clay, P. Dubois, M. Cosson, C. Jean-Charles, Biomechanical properties of vaginal tissue: preliminary results, International Urogynecology Journal 19 (2008) 811–816.

[10] B. Calvo, E. Peña, P. Martins, T. Mascarenhas, M. Doblaré, R. M. Natal Jorge, A. Ferreira, On modelling damage process in vaginal tissue., Journal of Biomechanics 42 (2009) 642–651.

[11] G. Chagnon, M. Rebouah, D. Favier, Hyperelastic Energy Densities for Soft Biological Tissues: A Review, Journal of Elasticity 120 (2015) 129–160.

[12] M. Brieu, P. Chantereau, J. Gillibert, L. de Landsheere, P. Lecomte, M. Cosson, A nonlinear-elastic constitutive model for soft connective tissue based on a histologic description: Application to female pelvic soft tissue., Journal of the mechanical behavior of biomedical materials 58 (2016) 65–74.

[13] P. Martins, E. Pena, N. R. M. Jorge, A. Santos, L. Santos, T. Mascarenhas, B. Calvo, Mechanical characterization and constitutive modelling of the damage process in rectus sheath, Journal of the Mechanical Behavior of Biomedical Materials 8 (2012) 111–122.

[14] G. M. Cooney, S. P. Lake, D. M. Thompson, R. M. Castile, D. C. Winter, C. K. Simms, Uniaxial and biaxial tensile stressstretch response of human linea alba 63 (2016) 134–140.

[15] C. Rubod, M. Brieu, M. Cosson, G. Rivaux, J.-C. Clay, L. de Landsheere, B. Gabriel, Biomechanical Properties of Human Pelvic Organs, Urology 79 (2012) 968.e17–968.e22.

[16] G. Huysmans, I. Verpoest, P. Van Houtte, A poly-inclusion approach for the elastic modelling of knitted fabric composites, Acta Mater. 46 (1998) 3003–3013.

[17] M. Duhovic, D. Bhattacharyya, Simulating the deformation mechanisms of knitted fabric composites, Composites - Part A: Applied Science and Manufacturing 37 (2006) 1897–1915.

[18] D. A. Chernous, S. V. Shil'ko, A. V. Charkovskii, A simplified description of the stress-strain state of a warp-knitted fabric, Mechanics of Composite Materials 46 (2010) 395–404.

[19] B. Gommers, I. Verpoest, P. Houtte, Modelling the elastic properties of knitted- fabric-reinforced composites, Compos. Sci. Technol. 56 (1996) 685–694.

[20] S. Ramakrishna, Characterization and modeling of the tensile properties of plain weft-knit fabric-reinforced composites, Composites Science and Technology 57 (1997) 1–22.

[21] G. Dusserre, L. Balea, G. Bernhart, Elastic properties prediction of a knitted composite with inlaid yarns subjected to stretching: A coupled semi-analytical model, Composites Part A: Applied Science and Manufacturing 64 (2014) 185–193.

[22] Z. M. Huang, S. Ramakrishna, A. Tay, Modeling the stress/strain behavior of a knitted fabric-reinforced elastomer composite, Composites Science and Technology 60 (2000) 671–691.

[23] M. Brieu, F. Devries, Homogénéisation de composites élastomères. Méthode et algorithme, Comptes Rendus de l'Académie des Sciences - Series IIb 326 (1998) 379–384.

[24] F. Devries, M. Brieu, Approche micro/macro de l'endommagement de milieux élastomères, Comptes Rendus de l'Académie des Sciences - Series IIb (1998) 905–910.

[25] N. Lahellec, F. Mazerolle, J. Michel, Second-order estimate of the macroscopic behavior of periodic hyperelastic composites: theory and experimental validation, Journal of the Mechanics and Physics of Solids 52 (2004) 27–49.
[26] M. Mooney, A theory of large elastic deformation, J. Appl. Phys. 11 (1940) 582–592.
[27] O. H. Yeoh, Some Forms of the Strain Energy Function for Rubber, Rubber Chemistry and Technology 66 (1993) 754–771.
[28] G. A. Holzapfel, T. C. Gasser, R. W. Ogden, Comparison of a Multi-Layer Structural Model for Arterial Walls With a Fung-Type Model, and Issues of Material Stability, Journal of Biomechanical Engineering 126 (2004) 264.
[29] T. C. Gasser, R. W. Ogden, G. A. Holzapfel, Hyperelastic modelling of arterial layers with distributed collagen fibre orientations., J. R. Soc. Interface 3 (2006) 15–35.
[30] M. S. Yeoman, D. Reddy, H. C. Bowles, D. Bezuidenhout, P. Zilla, T. Franz, A constitutive model for the warp-weft coupled non-linear behavior of knitted biomedical textiles, Biomaterials 31 (2010) 8484–8493.
[31] B. Hernández-Gascón, E. Peña, H. Melero, G. Pascual, M. Doblaré, M. P. Ginebra, J. M. Bellón, B. Calvo, Mechanical behaviour of synthetic surgical meshes: Finite element simulation of the herniated abdominal wall, Acta Biomaterialia 7 (2011) 3905–3913.
[32] A. J. Horbach, M. T. Duong, M. Staat, Modelling of compressible and orthotropic surgical mesh implants based on optical deformation measurement, Journal of the Mechanical Behavior of Biomedical Materials (2017).
[33] A. S. Milani, J. A. Nemes, An intelligent inverse method for characterization of textile reinforced thermoplastic composites using a hyperelastic constitutive model, Composites Science and Technology 64 (2004) 1565–1576.
[34] X. Peng, G. Guo, N. Zhao, An anisotropic hyperelastic constitutive model with shear interaction for cord-rubber composites, Composites Science and Technology 78 (2013) 69–74.
[35] Y. Gong, X. Peng, Y. Yao, Z. Guo, An anisotropic hyperelastic constitutive model for thermoplastic woven composite prepregs, Composites Science and Technology 128 (2016) 17–24.
[36] M. C. Wang, E. Guth, Statistical Theory of Networks of Non-Gaussian Flexible Chains, The Journal of Chemical Physics 20 (1952) 1144–1157.
[37] L. R. G. Treloar, G. Riding, A non-Gaussian theory for rubber in biaxial strain. I. Mechanical properties, Proc. R. Soc. Long. A 369 (1979) 261–280.
[38] E. M. Arruda, M. C. Boyce, A three-dimensional constitutive model for the large stretch behavior of rubber elastic materials, Journal of the Mechanics and Physics of Solids 41 (1993) 389–412.
[39] P. D. Wu, E. Van Der Giessen, On improved network models for rubber elasticity and their applications to orientation hardening in glassy polymers, Journal of the Mechanics and Physics of Solids 41 (1993) 427–456.
[40] C. Miehe, S. Göktepe, F. Lulei, A micro-macro approach to rubber-like materials - Part I: The non-affine micro-sphere model of rubber elasticity, Journal of the Mechanics and Physics of Solids 52 (2004) 2617–2660.
[41] J. Diani, M. Brieu, J.-M. Vacherand, A. Rezgui, Directional model for isotropic and anisotropic hyperelastic rubber-like materials, Mechanics of Materials 36 (2004) 313–321.
[42] Z. Bazant, B. Oh, Efficient numerical integration on the surface of a sphere, Zeitschrift für Angewandte Mathematik und Mechanik 66 (1986) 37–49.
[43] S. Heo, X. Yuan, Constructing fully symmetric cubature formulae for the sphere, Mathematics of Computation 70 (2001) 269–279.
[44] P. B. Badel, J. B. Leblond, A note on integration schemes for the microplane model of the mechanical behaviour of concrete, Communications in Numerical Methods in Engineering 20 (2004) 75–81.
[45] J. Gillibert, M. Brieu, J. Diani, Anisotropy of direction-based constitutive models for rubber-like materials, International Journal of Solids and Structures 47 (2010) 640–646.
[46] A. Menzel, P. Steinmann, A theoretical and computational framework for anisotropic continuum damage mechanics at large strains, International Journal of Solids and Structures 38 (2001) 9505–9523.
[47] S. Göktepe, C. Miehe, A micro-macro approach to rubber-like materials. Part III: The micro-sphere model of anisotropic Mullins-type damage, Journal of the Mechanics and Physics of Solids 53 (2005) 2259–2283.
[48] J. Diani, M. Brieu, J.-M. Vacherand, A damage directional constitutive model for Mullins effect with permanent set and induced anisotropy, European Journal of Mechanics, A/Solids 25 (2006) 483–496.
[49] M. Itskov, A. Knyazeva, A rubber elasticity and softening model based on chain length statistics, International Journal of Solids and Structures 80 (2016) 512–519.
[50] A. Raina, C. Linder, A homogenization approach for nonwoven materials based on fiber undulations and reorientation, Journal of the Mechanics and Physics of Solids 65 (2014) 12–34.
[51] E. Kuhl, K. Garikipati, E. M. Arruda, K. Grosh, Remodeling of biological tissue: Mechanically induced reorientation of a transversely isotropic chain network, Journal of the Mechanics and Physics of Solids 53 (2005) 1552–1573.
[52] A. Menzel, T. Waffenschmidt, A microsphere-based remodelling formulation for anisotropic biological tissues, Philosophical Transactions of the Royal Society A: Mathematical, Physical and Engineering Sciences 367 (2009) 3499–3523.
[53] V. Alastrué, M. A. Martínez, M. Doblaré, A. Menzel, Anisotropic micro-sphere-based finite elasticity applied to blood vessel modelling, Journal of the Mechanics and Physics of Solids 57 (2009) 178–203.
[54] P. Sáez, E. Peña, M. Ángel Martínez, E. Kuhl, Mathematical modeling of collagen turnover in biological tissue, Journal of Mathematical Biology 67 (2013) 1765–1793.
[55] V. Alastrué, P. Sáez, M. A. Martínez, M. Doblaré, On the use of the Bingham statistical distribution in microsphere-based constitutive models for arterial tissue, Mechanics Research Communications 37 (2010) 700–706.
[56] P. Sáez, V. Alastrué, E. Peña, M. Doblaré, M. A. Martínez, Anisotropic microsphere-based approach to damage in soft fibered tissue, Biomechanics and Modeling in Mechanobiology 11 (2012) 595–608.
[57] NF-EN 5084, Textiles - détermination de l'épaisseur des textiles et produits textiles, 1996.
[58] NF-EN 13934-1, Textiles - Propriétés des étoffes en traction - Partie 1 : détermination de la force maximale et de

l'allongement à la force maximale par la méthode sur bande, 2013.
[59] A. Morch, B. Pouseele, G. Doucède, J.-F. Witz, F. Lesaffre, P. Lecomte-Grosbras, M. Brieu, M. Cosson, C. Rubod, Experimental study of the mechanical behavior of an explanted mesh: The influence of healing, Journal of the Mechanical Behavior of Biomedical Materials 65 (2017) 190–199.
[60] L. Mullins, Effect of Stretching on the Properties of Rubber, 1948. doi:10.5254/1.3546914.
[61] J. Diani, M. Brieu, P. Gilormini, Observation and modeling of the anisotropic visco-hyperelastic behavior of a rubberlike material, Int. J. Solids Struct. 43 (2006) 3044–3056.
[62] W. Kuhn, F. Grün, Beziehungen zwischen elastischen Konstanten und Dehnungsdoppelbrechung hochelastischer Stoffe, Kolloid-Zeitschrift 101 (1942) 248–271.
[63] A. Cohen, A Padé approximant to the inverse Langevin function, Rheologica Acta 30 (1991) 270–273.
[64] I. Carol, M. Jirásek, Z. P. Bažant, A framework for microplane models at large strain, with application to hyperelasticity, International Journal of Solids and Structures 41 (2004) 511–557.
[65] A. Lion, N. Diercks, J. Caillard, On the directional approach in constitutive modelling: A general thermomechanical framework and exact solutions for Mooney-Rivlin type elasticity in each direction, International Journal of Solids and Structures 50 (2013) 2518–2526.
[66] R. Storn, K. Price, Differential Evolution A Simple and Efficient Heuristic for global Optimization over Continuous Spaces, Journal of Global Optimization 11 (1997) 341–359.
[67] E. Jones, T. Oliphant, P. Peterson, SciPy : Open source scientific tools for Python, 2001. URL: http://www.scipy.org/.
[68] T. E. Oliphant, A guide to NumPy, 2006.